ACS APPLIED MATERIALS & INTERFACES

Forum Article

www.acsami.org

AC Measurements Using Organic Electrochemical Transistors for Accurate Sensing

Naixiang Wang, Yuzhe Liu, Ying Fu, and Feng Yan*

Department of Applied Physics, The Hong Kong Polytechnic University, Hong Kong

Supporting Information

ABSTRACT: Organic electrochemical transistors (OECTs) have been successfully employed for a variety of applications , especially chemical and biological sensing. Although the device response to analytes can be directly monitored by measuring steady-state channel currents of the devices, it is challenging to obtain stable signals with high signal-to-noise ratios. In this work, we developed a novel method for electrochemical sensing by measuring both the transconductance and the phase of the AC channel current for the first time. Then we successfully realized highly sensitive ion strength sensors and dopamine sensors based on the AC method. Our results indicate that the AC method is more sensitive than typical DC methods and can provide more stable data in sensing applications. Considering that the sensors can be conveniently integrated with AC circuits, this technology is expected to find broad applications in the future.

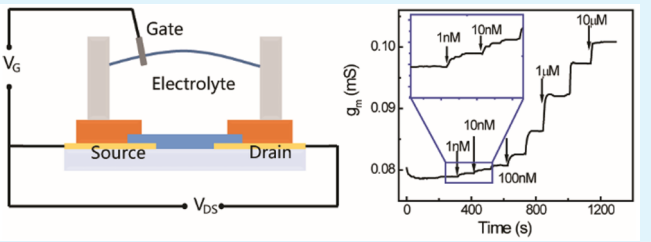

KEYWORDS: *organic electrochemical transistor, organic semiconductor, AC method, biosensor, dopamine sensor, thin film transistor*

1. INTRODUCTION

Organic electrochemical transistors (OECTs), a kind of organic thin film transistors operating in aqueous electrolytes, have exhibited great potential for the applications as biosensors.[1,2] Since the demonstration of the first OECT in 1984,[3] it has been extensively investigated as a promising platform for a wide range of chemical and biological sensing applications, including ions,[4−7] pH,[8] glucose,[9,10] dopamine,[11,12] bacteria,[13] cells,[14−16] and tissues,[17−20] etc. A figure of merit for a biosensor is the limit of detection (LOD), which is determined by the signal-to-noise ratio that normally should be higher than 3.[21,22] Therefore, an effective method for optimizing the LOD of a device is to decrease the noise level in the measurement. The characterization of various OECT-based biosensors reported before is mainly based on the measurement of DC current responses of the devices to analytes and the LODs of the devices are decided at the analyte concentrations when the DC current responses are 3 times higher than the noise levels of the channel currents.

AC measurements can effectively alleviate noise by filter circuits and lead to more stable data than DC approaches, which, however, have been rarely reported before. The major reason is due to the long response times (normally ∼10 s) of OECTs to external signals. In 2013, Khodagholy et al.[23] reported the fabrication of high-speed OECT arrays with small device sizes and performed a detailed investigation into the steady-state and transient-state characteristics of the OECTs, indicating the possibility to operate the devices at a frequency of up to several kilohertz for sensing applications. Tybrandt et al. successfully integrated OECT into fast scan cyclic voltammetry for on-site amplification application to characterize the concentration of dopamine.[24] Then in 2015, Rivnay et al.[25] developed a new technique to combine OECT drain current measurement with simultaneous traditional impedance sensing, for in vitro cell based sensing. Ramuz et al.[26] also showed the possibility to use transconductance-frequency spectrum for monitoring of cell layer coverage and differentiation, indicating the advantage of AC characterization in noninvasive dynamic assessment of the integrity of cells. More recently, Gualandi et al.[27] introduced a potential dynamic approach into an all-PEDOT OECT sensor used for dopamine detection, which shows high selectivity to interferences by separating the redox waves of the transconductance curves for each compound. However, the introduction of AC measurements of OECTs in electrochemical sensing has not yet been systematically investigated until now.

In this work, we demonstrate AC measurements of OECT-based biosensors that can detect ion strength and chemicals (i.e., dopamine) with lower LODs. By miniaturizing the channel area of OECT to tens of micrometers, the device response time could be decreased to 10^{-5} s. Compared with conventional sensing methods based on measuring DC channel currents, the AC method shows several advantages, such as more information available (both amplitude and phase of channel currents), more stable signal, and higher signal-to-noise

Special Issue: Materials and Interfaces for Next Generation Thin Film Transistors

Received: May 30, 2017
Accepted: August 17, 2017

DOI: 10.1021/acsami.7b07668
ACS Appl. Mater. Interfaces XXXX, XXX, XXX−XXX

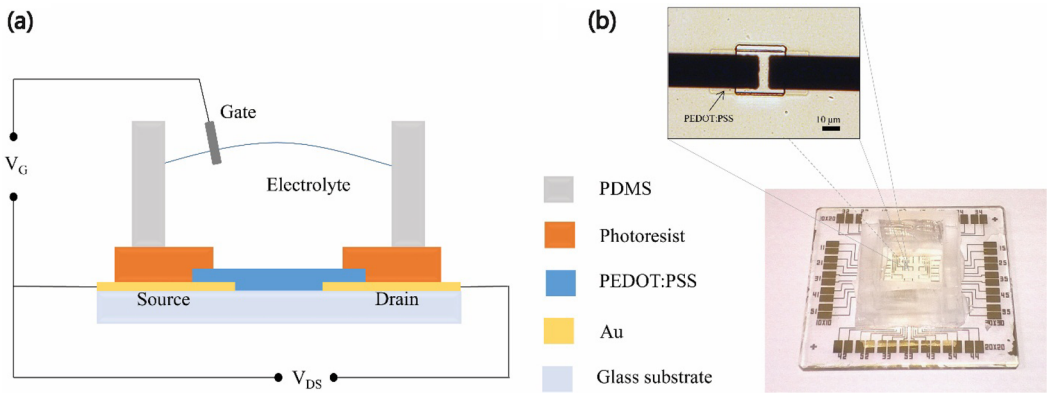

Figure 1. Structure of the OECT. (a) Schematic diagram of an OECT cross-section and the wiring system for device operation. (b) Optical micrograph of an individual transistor and the whole OECT array.

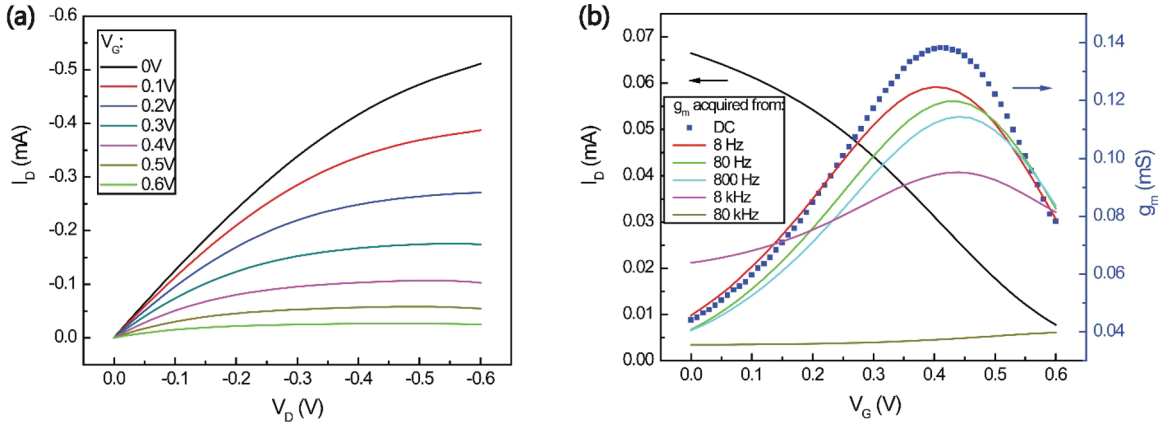

Figure 2. (a) Output characteristics (drain current I_D versus drain voltage V_D) of an OECT under gate voltage V_G varying from 0 to 0.6 V. (b) Transfer curve (black line, $I_D \sim V_G$) and resulting transconductance (blue symbols) derived from mathematical differential at V_D = 0.05 V, together with transconductance curves derived from AC sweeping of g_m over V_G bias under various measurement frequencies (from 8 Hz to 80 kHz).

ratio. Therefore, the devices characterized with AC measurements would be very useful in the applications as bioelectronics.

2. EXPERIMENTAL SECTION

2.1. Materials. Poly(3,4-ethylenedioxythiophene)−poly(styrenesulfonate) (PEDOT:PSS) (Clevios PH-500) aqueous solution was purchased from Heraeus Ltd.. Phosphate buffered saline (PBS) solution (pH 7.4), dimethyl sulfoxide (DMSO), glycerin, and dopamine were all purchased from Sigma-Aldrich Co. and stored at 4 °C for further use. (3-Glycidyloxypropyl)trimethoxysilane (GOPS) was purchased from International Laboratory, USA. AZ5214 and SU-8 2002 photoresists were purchased from Microchemicals GmbH.

2.2. Device Fabrication. We developed a novel, convenient, and reproducible approach to prepare OECTs by multilayer photolithography. The device architecture of an OECT is illustrated in Figure 1. The fabrication process of OECT included the deposition and patterning of metal electrode, PEDOT:PSS layer, and photoresist insulating layer in sequence (Supporting Information Figure S1). Glass substrates were surface polished and cleaned by chemical and plasma methods. AZ5214 photoresist was spin coated and exposed to UV light using OAI 800 contact aligner and then developed by AZ 400K developer. Then Au (~100 nm)/Cr (~10 nm) electrodes were deposited on the glass substrate by magnetron sputtering through a standard lift-off process. The channel length (L) and width (W) of the devices were 5 and 22 μm, respectively (Figure 1b). Then a second layer of photoresist was spin coated on the substrate with electrodes, and the channel window was opened by alignment photolithography. For the preparation of PEDOT:PSS film, the aqueous dispersion was mixed with DMSO and glycerin (both with a volume ratio of 5%) to improve the conductivity and stability of PEDOT:PSS films. In addition, the cross-linker GOPS was added to the above dispersion with a volume ratio of 1% to prohibit PEDOT:PSS dissolution. PEDOT:PSS was then spin coated on the patterned photoresist and annealed at 150 °C for 1 h. After that, unwanted PEDOT:PSS with photoresist were removed by washing with acetone. At last, another layer of SU-8 2002 photoresist was spin coated and patterned on the surface of the PEDOT:PSS film, acting as an insulating layer to protect the Au electrodes from the aqueous electrolyte. The surface morphology of PEDOT:PSS films before and after the photolithography processes were investigated by atomic force microscopy, as shown in Figure S2. No difference can be observed in the surface morphology and roughness before and after the photolithography processes, indicating that the PEDOT:PSS layer is very stable during the device fabrication. Devices were subsequently immersed in PBS buffer solution to remove any excess of low molecular weight compounds. At last a reservoir made of a poly(dimethylsiloxane) (PDMS) wall was attached to the substrate to form the aqueous electrolyte containing cell for characterization and sensing application of the devices. The gate electrode of OECT was deposited separately by magnetron sputtering through a shadow mask, resulting in a 3 mm × 3 mm patterned Ti (~10 nm)/Pt (~100 nm) electrode. Then the electrode was immersed into the PBS solution in the PDMS well for electrical characterization.

2.3. Device Characterization. The OECT device was immersed in PBS buffer solution, as shown in Figure 1a. The optical images of the device were observed by Olympus IX71 inverted microscope. The output and transfer characteristics of the devices were measured by two Keithley source meters (Keithley 2400). For transient measurements, an Agilent 33220A waveform generator was used to provide the

DOI: 10.1021/acsami.7b07668
ACS Appl. Mater. Interfaces XXXX, XXX, XXX−XXX

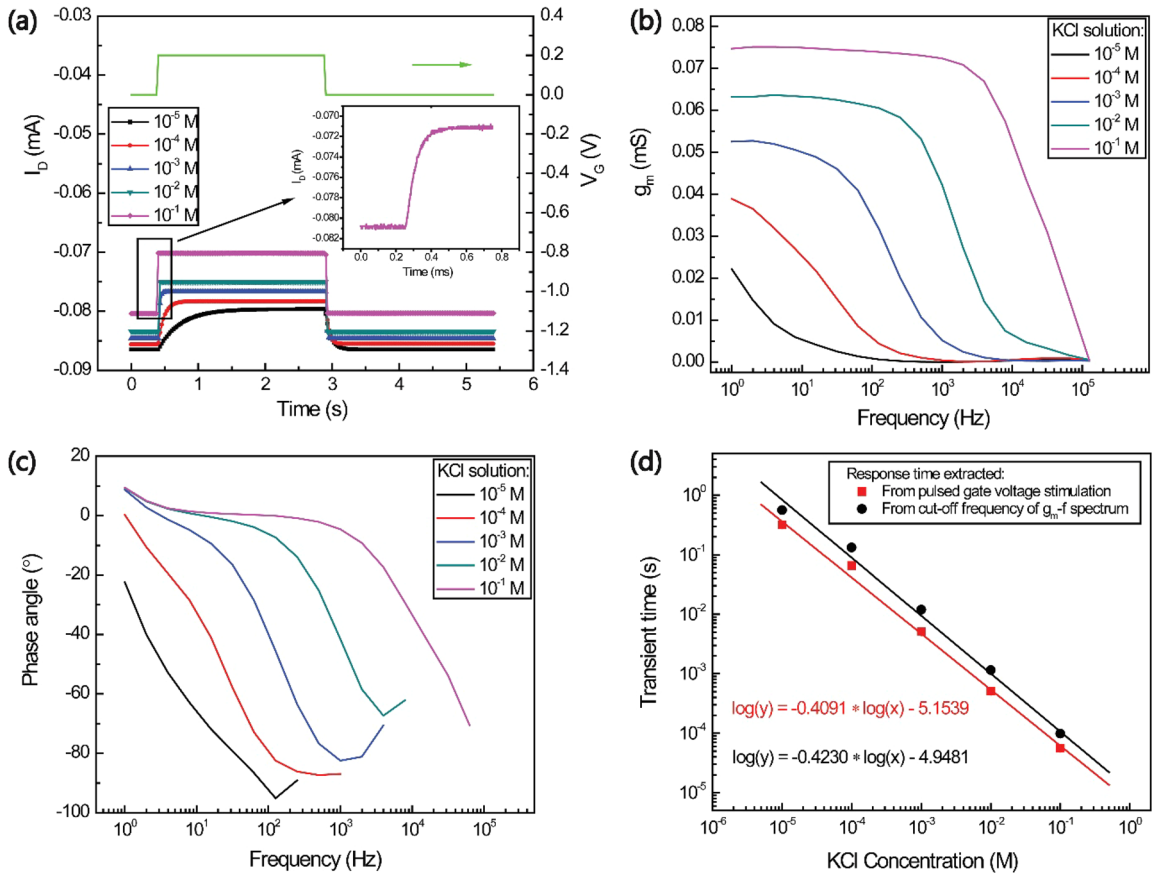

Figure 3. (a) Channel current response to a V_G pulse of 0.2 V, with a drain voltage of V_D = 0.05 V, for an OECT operated in a series of KCl solutions with increasing concentration from 10^{-5} to 10^{-1} M. Inset: Channel current response of a device operated in 10^{-1} M KCl solution, with the time axis in the millisecond range. (b) Frequency dependence of the small signal transconductance value and (c) corresponding phase angle under various ionic concentrations of KCl. The device is biased with V_D = 0.05 V and V_G = 0.2 V. (d) Extracted time constant from pulsed gate voltage stimulation (red) and cutoff frequency of g_m frequency spectrum (black) as a function of KCl concentration. The lines are for double-log linear fitting.

gate voltage pulse, and the channel current response was recorded by the Tektronix TDS2000C digital storage oscilloscope. For the small signal transconductance measurement, the sinusoids gate input (with the amplitude of 50 mV and a certain bias) was applied by the waveform generator, and the drain current was converted by SR570 low noise current preamplifier into a voltage signal and then collected by the SR830 DSP lock-in amplifier, to get the transconductance and the corresponding phase angle shift. The instruments were connected and controlled by a customized LabVIEW program. To demonstrate the advantages of the AC measurements, OECT-based ion sensors and dopamine sensors were characterized under AC gate voltages. In the measurement, dopamine aqueous solutions (diluted with PBS) with designed concentrations were added into the PBS solution in the PDMS reservoir and mixed by a pipet to measure the change of transconductance at a fixed gate voltage.

3. RESULTS AND DISCUSSION

3.1. AC Measurements. Figure 2a shows the output characteristics of a typical OECT with negative sweeping bias (0 to −0.6 V) on the drain and stepped gate voltages varied from 0 to 0.6 V applied from the Pt gate electrode immersed into the PBS solution. The corresponding transfer curve for V_D = 0.05 V is shown in Figure 2b. The drain current decreases with the increasing gate voltage, showing the typical low-voltage operation of OECT in the depletion regime.[28] The transconductance ($g_m = \Delta I_D/\Delta V_G$) derived from the transfer curve (blue symbols in Figure 2b) reaches a peak value of g_m = 0.138 mS at V_G = 0.41 V. It is notable that the simultaneously measured gate current (leakage) of the devices is less than 30 nA throughout the output and transfer characterization (Figure S3), demonstrating the good insulation performance of the SU-8 photoresist layer used to package the source and drain electrodes.

Next, the device was characterized with an AC method. A small sinusoidal oscillation signal (v_g, 50 mV in amplitude) with the frequency of f is superimposed on the gate bias V_G, leading to an AC channel current of OECT. The AC gate voltage v_G and the induced channel current i_{DS} (consists of DC component I_{DS} and AC component i_{ds}) are given by

$$\begin{aligned} v_G &= V_G + v_g = V_G + |v_g|e^{j2\pi ft} \\ i_{DS} &= I_{DS} + i_{ds} = I_{DS} + |i_{ds}|e^{j(2\pi ft+\theta)} \end{aligned} \quad (1)$$

Then the transconductance is defined as

$$g_m = \left.\frac{\Delta i_{DS}}{\Delta v_G}\right|_{V_{DS}} = \frac{|i_{ds}|}{|v_g|}e^{j\theta} \quad (2)$$

Therefore, by superimposing a small sinusoidal signal (with fixed amplitude $|v_g|$) to the gate voltage, the transconductance g_m with corresponding phase shift angle θ could be collected simultaneously by the lock-in amplifier.

DOI: 10.1021/acsami.7b07668
ACS Appl. Mater. Interfaces XXXX, XXX, XXX−XXX

By simply sweeping V_G from 0 to 0.6 V, the $g_m - V_G$ relations under different operation frequencies were obtained, as shown in Figure 2b. It is reasonable that when operated at relatively low frequencies, the transconductance curves are quite similar to the one derived from the transfer characterization at steady state, all reaching a peak value at around $V_G = 0.41$ V. With the increase of the operation frequency from 8 Hz to 80 kHz, the peak value decreases due to the lagged response of the ions moving between the aqueous electrolyte and the PEDOT:PSS channel.

3.2. Ion Strength Sensing by OECTs. Although OECTs have been successfully employed in various kinds of sensing applications, a major drawback of the devices is the slow device response. According to the device physics of OECTs,[23,25] the drain current of a device is dependent on the number of ions that could be injected into the channel, which in turn determines the time needed for the device to reach the steady state. We consider that the device response speed is closely related to the ion concentrations. Therefore, the dynamic response of OECTs is expected to imply the ion concentrations in the electrolytes and, consequently, ion strength sensors can be realized based on this principle.

To characterize the effect of ion strength on the response speed, the transient behavior of an OECT under the application of a gate voltage was measured first. Here, a gate voltage pulse ($V_G = 0.2$ V) is applied through the electrolyte with various KCl concentrations, as shown in Figure 3a. The channel current I_D is monitored simultaneously with the applied pulsed V_G. When V_G was switched from 0 to 0.2 V, a rapid decrease of I_D was observed, followed by nearly steady state behavior after a certain period of time. According to the Bernards' model[28] and further investigation by Friedlein et al.,[29]

$$I_D(t) = I_D(0) + \Delta I_D[1 - \exp(-t/\tau_{RC})] \tag{3}$$

The ionic RC time constant τ_{RC} is the key factor limiting the response speed of the device. Then a first order exponential decay ($I_D(t) \sim \exp(-t/\tau_{RC})$) is applied on the fitting of the responding drain current curve in Figure 3a to extract the transient response time τ_{RC}. Then this response time is plotted as a function of the KCl concentration and a linear fitting is applied on the double-log axis in Figure 3d. The response time is shortened by 4 orders of magnitude, from 0.32 to 5.58×10^{-5} s, as the result of increasing KCl concentration from 10^{-5} to 10^{-1} M. The result indicates that the response time has a good linear relationship with the ion concentrations in electrolytes, under a log–log plot, indicating that the response time of OECT can be used to identify the ion concentrations in the electrolytes. By fitting the data in Figure 3d, the relationship between the response time and the ion concentration can be presented in the following power function:

$$\tau_{RC} = 10^{-5.15} {c_{ion}}^{-0.409} \tag{4}$$

where c_{ion} represents the ion concentration in an electrolyte.

It is more convenient to characterize the response time of a device by AC measurements. The frequency-dependent transconductance was characterized in electrolytes with different ion concentrations. Figure 3b shows the tendency of g_m versus KCl concentration in the frequency range from 1 to 10^5 Hz. The corresponding phase angle shift is also shown in Figure 3c. When the ion concentration is higher than 10^{-3} M, the phase angle keeps at a constant value in the low-frequency region, and only the shift of the curves along the x-axis could be observed for varying concentrations.

The decrease of g_m with increasing frequency here provides another method to extract the response time of the OECT device. The cutoff frequency is defined at the point when the g_m value decreases to 0.707 of the maximum value (−3 dB).[30,31] So the response time is the reciprocal of the cutoff frequency, and again the relationship between the response time and the concentration is plotted in Figure 3d. By fitting the experimental results, we can get the following power function relation between response time and ion concentration, which is similar to that obtained from the transient measurements.

$$\tau_{RC} = 10^{-4.95} {c_{ion}}^{-0.423} \tag{5}$$

Therefore, both the transient and the AC methods can be used to characterize the response time of an OECT and used to decide the ion concentrations in electrolytes.

According to previous investigation by Khodagholy et al.,[23] the response time of OECT is majorly limited by the ion transport in the ionic circuit (between the aqueous electrolyte and PEDOT:PSS film), considering that the hole transport in the PEDOT:PSS channel is a much faster step. Therefore, this relationship between the response time and the ionic concentration could be explained by simplifying the ionic circuit as a resistor (with the resistance R) and capacitor (with the capacitance C) in series. According to the definition, the conductance G of the electrolyte solution is given by

$$G = \frac{1}{R} = \kappa\frac{A}{l} = \Lambda_m c_{ion}\frac{A}{l} \tag{6}$$

where κ is the electrolyte conductivity, l and A are the length and the cross-section area of the ionic circuit, and Λ_m represents the molar conductivity. Therefore, the resistance is given by

$$R = \frac{l}{\Lambda_m c_{ion} A} \tag{7}$$

For the discussion of capacitance in PEDOT:PSS film, recently Proctor et al.[32] carried out a simple model by describing the capacitance in terms of the sites where holes are replaced by the ions injected from the electrolyte. Therefore, the capacitance per unit volume, which is called the volumetric capacitance C^*, is given by

$$C^* = \frac{C'_{DL}}{\alpha} \tag{8}$$

where C'_{DL} is the conventional double layer capacitance from the Helmholtz model and α is the average distance between sites. The volumetric capacitance could then be further derived,

$$C^* = \frac{C'_{DL}}{\alpha} = \frac{\varepsilon_0\varepsilon_r}{d}\frac{1}{\alpha} = \frac{\varepsilon_0\varepsilon_r}{\frac{1}{F}\sqrt{\frac{R_g T\varepsilon_0\varepsilon_r}{2c_{ion}}}}\frac{1}{\alpha} = \frac{F}{\alpha}\sqrt{\frac{2c_{ion}}{R_g T\varepsilon_0\varepsilon_r}} \tag{9}$$

where ε_0 and ε_r are the vacuum and relative permittivity, d is the thickness of the electric double layer, F is the Faradaic constant, R_g is the gas constant, and T is the absolute temperature. Then the response time is given by the RC time of the circuit:[33]

$$\tau_{RC} = RC^* = \frac{l}{\Lambda_m c_{ion} A}\frac{F}{\alpha}\sqrt{\frac{2c_{ion}}{R_g T\varepsilon_0\varepsilon_r}} = \frac{lF}{\alpha\Lambda_m A}\sqrt{\frac{2}{R_g T\varepsilon_0\varepsilon_r}}\,{c_{ion}}^{-1/2} \tag{10}$$

DOI: 10.1021/acsami.7b07668
ACS Appl. Mater. Interfaces XXXX, XXX, XXX−XXX

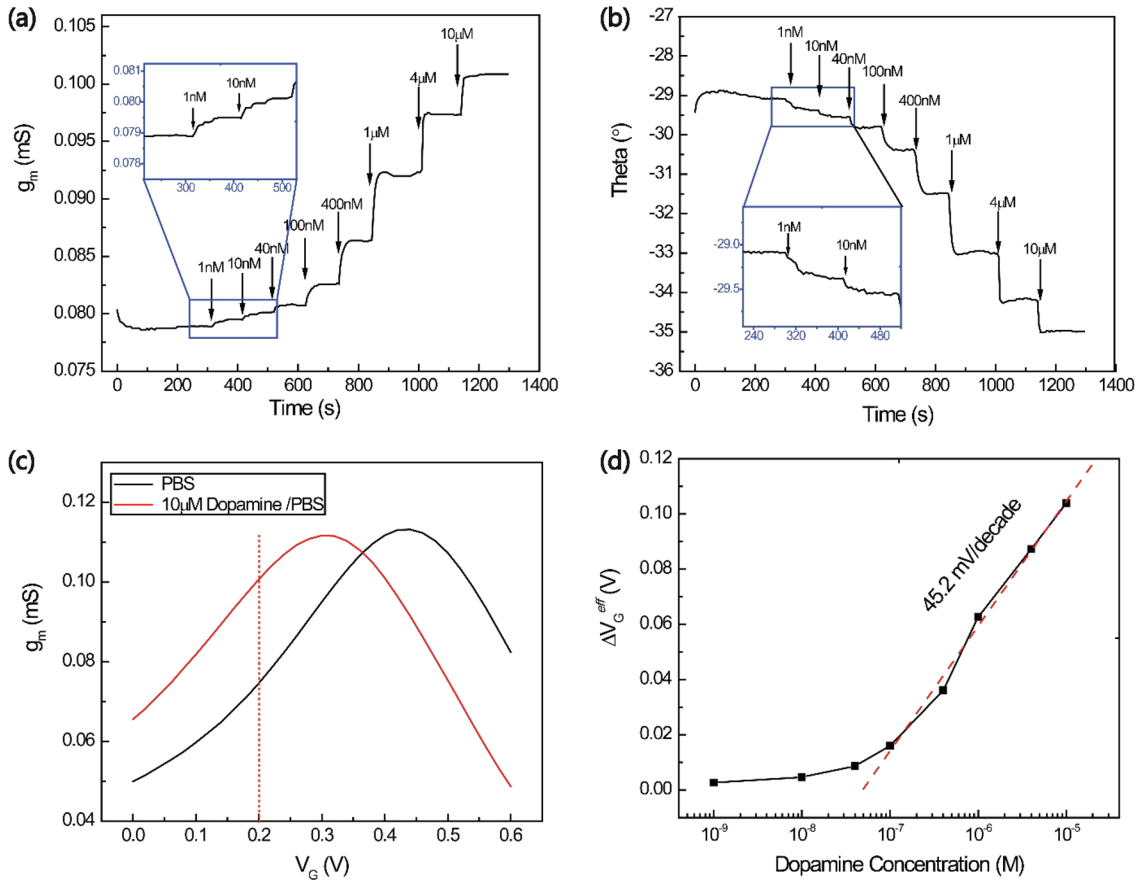

Figure 4. (a) Channel transconductance (g_m) response and (b) associated phase angle change of the OECT to additions of dopamine with different concentrations. V_D = 0.05 V; V_G = 0.2 V. (c) V_G dependent transconductance (g_m versus V_G, V_{DS} = 0.05 V) of an OECT measured in PBS solution (pH = 7.4) before and after the addition of dopamine with the concentration of 10 μM. (d) Change of effective gate voltage (ΔV_G^{eff}) as a function of dopamine concentration.

This equation indicates that, under an optimum condition, the time constant τ_{RC} is proportional to $c_{ion}^{-1/2}$. The experimental results from both the transient and the AC measurements show the same power function relationship between τ_{RC} and c_{ion} with the exponent of around −0.41. This can be ascribed to the fact that the molar conductivity Λ_m is also concentration dependent (in diluted solution, Λ_m decreases with increasing ionic concentration). For the concentration varying in such a wide range, deviation from the idealized model may be present.

3.3. Dopamine Sensors. It is expected that AC measurements of OECT-based biosensors can lead to better sensitivity and LOD since the noise levels of the devices can be greatly decreased by filters. Therefore, we developed an AC method for characterizing an OECT-based dopamine sensor. As reported before, an OECT with Pt gate electrode is sensitive to dopamine in solution because the reaction of dopamine at the Pt gate electrode may modulate the effective gate voltage V_G^{eff} applied on the device and the relationship between V_G^{eff} and the concentration of dopamine [$C_{dopamine}$] is given by[11]

$$V_G^{eff} = V_G + 2.30(1+\gamma)\frac{kT}{2q}\log[C_{dopamine}] + a \quad (11)$$

where γ is the capacitance ratio, defined as C_C/C_G, in which C_C and C_G are the channel/electrolyte capacitance and gate/electrolyte capacitance, respectively; k is the Boltzmann's constant, T is the temperature, and a is a constant. Moreover, since g_m changes with the gate voltage, different concentrations of dopamine can lead to the change of g_m of the device. Based on this principle, an OECT was characterized by AC measurements in PBS solution with the addition of dopamine with different concentrations. Both the transconductance g_m and the phase of the device were characterized simultaneously, as shown in Figure 4.

During the measurements, V_D = 0.05 V and V_G = 0.2 V with the addition of 50 mV sinusoidal signal were applied on the device and the response of the OECT to continuous addition of dopamine is reflected by the real-time response of both g_m and phase angle. As shown in Figure 4a, the device starts to exhibit an obvious signal response to the addition of 1 nM dopamine, which is lower than the LOD of DC measurements previously reported.[11,34] A DC measurement was also carried out (shown in Figure S4) with the same device, and LOD could only reach 10 nM. The DC response of the device to the addition of 1 nM is not obvious in comparison with the variation of the channel current under constant voltages.

Further into the mechanism, the change of g_m and θ can be attributed to the change of effective gate voltage due to the oxidation reaction of dopamine at the surface of the Pt gate electrode. This will further result in the horizontal shift of the g_m−V_G curve. As indicated in Figure 4c, the curve shows a shift of about 150 mV to lower gate voltage when the device is characterized in 10 μM dopamine PBS solution, compared to the blank PBS solution. The same behavior is observed for the θ−V_G curve (Figure S5). By addition of 10 μM dopamine, a

DOI: 10.1021/acsami.7b07668
ACS Appl. Mater. Interfaces XXXX, XXX, XXX−XXX

shift to lower gate voltage is also available due to the change of effective gate voltage. This could explain the similar response of g_m and θ to the addition of dopamine solution, as shown in Figure 4a,b.

Figure 4d shows the relationship between the variation of ΔV_G^{eff} and $[C_{dopamine}]$. We can find that ΔV_G^{eff} is proportional to $\log[C_{dopamine}]$ in the range of 1×10^{-7} to 1×10^{-5} M, across 2 orders of magnitude, which is consistent with eq 11. The slope value (45.2 mV/decade) of the fitting curve (dashed line in Figure 4d) indicates the response of the device toward the target analyte and could also be used to derive the capacitance ratio $\gamma = 0.53$ in eq 11. The relatively small value of γ can be explained by the influence of device geometry, according to the definition

$$\gamma = \frac{C_{channel}}{C_{gate}} = \frac{c_{ch}A_{ch}}{c_g A_g} \quad (12)$$

where c_{ch} and c_g are the channel and gate capacitances per unit area and A_{ch} and A_g are the areas of channel and gate electrode, respectively. The capacitance ratio is tunable and proportional to A_{ch}/A_g. As we patterned the channel area into tens of micrometer size by photolithography, A_{ch}/A_g is significantly reduced, which then decreases the value of γ, and consequently the slope of the fitting curve in Figure 4d.

4. CONCLUSIONS

In conclusion, we have systematically developed AC measurements for OECT-based biosensors. The AC method could be introduced to characterize not only the behavior of ionic motion and the ion concentrations in aqueous electrolytes but also an electrochemical sensing process for highly sensitive (detection limit down to 1 nM) and rapid detection of dopamine. The main advantages of the AC method over a traditional DC method include the ability to collect a more stable and accurate signal in a broad frequency range and the low noise level by introducing a lock-in amplifier. Therefore, the AC method would be a promising approach for further applications of OECTs in a noisy environment and complex biological systems.

■ ASSOCIATED CONTENT

Supporting Information

The Supporting Information is available free of charge on the ACS Publications website at DOI: 10.1021/acsami.7b07668.

Device fabrication procedure; AFM characterization of PEDOT:PSS films; gate leakage of a representative device; DC measurement for comparison; and phase angle curves measured in PBS and dopamine solution (PDF)

■ AUTHOR INFORMATION

Corresponding Author

*E-mail: apafyan@polyu.edu.hk.

ORCID

Feng Yan: 0000-0001-7385-6334

Notes

The authors declare no competing financial interest.

■ ACKNOWLEDGMENTS

This work was financially supported by the Research Grants Council (RGC) of Hong Kong, China (Project No. C5015-15G), and the Hong Kong Polytechnic University (Project No. G-SB51).

■ REFERENCES

(1) Owens, R. M.; Malliaras, G. G. Organic Electronics at the Interface with Biology. *MRS Bull.* **2010**, *35*, 449−456.
(2) Tarabella, G.; Mahvash Mohammadi, F.; Coppede, N.; Barbero, F.; Iannotta, S.; Santato, C.; Cicoira, F. New Opportunities for Organic Electronics and Bioelectronics: Ions in Action. *Chem. Sci.* **2013**, *4*, 1395−1409.
(3) White, H. S.; Kittlesen, G. P.; Wrighton, M. S. Chemical Derivatization of an Array of Three Gold Microelectrodes with Polypyrrole: Fabrication of a Molecule-Based Transistor. *J. Am. Chem. Soc.* **1984**, *106*, 5375−5377.
(4) Lin, P.; Yan, F.; Chan, H. L. W. Ion-Sensitive Properties of Organic Electrochemical Transistors. *ACS Appl. Mater. Interfaces* **2010**, *2*, 1637−1641.
(5) Sessolo, M.; Rivnay, J.; Bandiello, E.; Malliaras, G. G.; Bolink, H. J. Ion-Selective Organic Electrochemical Transistors. *Adv. Mater.* **2014**, *26*, 4803−4807.
(6) Yi, Z.; Natale, G.; Kumar, P.; Di Mauro, E.; Heuzey, M.-C.; Soavi, F.; Perepichka, I. I.; Varshney, S. K.; Santato, C.; Cicoira, F. Ionic Liquid−water Mixtures and Ion Gels as Electrolytes for Organic Electrochemical Transistors. *J. Mater. Chem. C* **2015**, *3*, 6549−6553.
(7) Kumar, P.; Yi, Z. H.; Zhang, S. M.; Sekar, A.; Soavi, F.; Cicoira, F. Effect of Channel Thickness, Electrolyte Ions, and Dissolved Oxygen on the Performance of Organic Electrochemical Transistors. *Appl. Phys. Lett.* **2015**, *107*, 053303.
(8) Nishizawa, M.; Matsue, T.; Uchida, I. Penicillin Sensor Based on a Microarray Electrode Coated with pH-Responsive Polypyrrole. *Anal. Chem.* **1992**, *64*, 2642−2644.
(9) Tang, H.; Yan, F.; Lin, P.; Xu, J. B.; Chan, H. L. W. Highly Sensitive Glucose Biosensors Based on Organic Electrochemical Transistors Using Platinum Gate Electrodes Modified with Enzyme and Nanomaterials. *Adv. Funct. Mater.* **2011**, *21*, 2264−2272.
(10) Zhang, M.; Liao, C.; Mak, C. H.; You, P.; Mak, C. L.; Yan, F. Highly Sensitive Glucose Sensors Based on Enzyme-Modified Whole-Graphene Solution-Gated Transistors. *Sci. Rep.* **2015**, *5*, 8311.
(11) Tang, H.; Lin, P.; Chan, H. L. W.; Yan, F. Highly Sensitive Dopamine Biosensors Based on Organic Electrochemical Transistors. *Biosens. Bioelectron.* **2011**, *26*, 4559−4563.
(12) Casalini, S.; Leonardi, F.; Cramer, T.; Biscarini, F. Organic Field-Effect Transistor for Label-Free Dopamine Sensing. *Org. Electron.* **2013**, *14*, 156−163.
(13) He, R.-X.; Zhang, M.; Tan, F.; Leung, P. H. M.; Zhao, X.-Z.; Chan, H. L. W.; Yang, M.; Yan, F. Detection of Bacteria with Organic Electrochemical Transistors. *J. Mater. Chem.* **2012**, *22*, 22072−22076.
(14) Lin, P.; Yan, F.; Yu, J.; Chan, H. L. W.; Yang, M. The Application of Organic Electrochemical Transistors in Cell-Based Biosensors. *Adv. Mater.* **2010**, *22*, 3655−3660.
(15) Bolin, M. H.; Svennersten, K.; Nilsson, D.; Sawatdee, A.; Jager, E. W. H.; Richter-Dahlfors, A.; Berggren, M. Active Control of Epithelial Cell-Density Gradients Grown along the Channel of an Organic Electrochemical Transistor. *Adv. Mater.* **2009**, *21*, 4379−4382.
(16) Gu, X.; Yao, C.; Liu, Y.; Hsing, I.-M. 16-Channel Organic Electrochemical Transistor Array for In Vitro Conduction Mapping of Cardiac Action Potential. *Adv. Healthcare Mater.* **2016**, *5*, 2345−2351.
(17) Jimison, L. H.; Tria, S. A.; Khodagholy, D.; Gurfinkel, M.; Lanzarini, E.; Hama, A.; Malliaras, G. G.; Owens, R. M. Measurement of Barrier Tissue Integrity with an Organic Electrochemical Transistor. *Adv. Mater.* **2012**, *24*, 5919−5923.
(18) Khodagholy, D.; Doublet, T.; Quilichini, P.; Gurfinkel, M.; Leleux, P.; Ghestem, A.; Ismailova, E.; Hervé, T.; Sanaur, S.; Bernard, C.; Malliaras, G. G. In Vivo Recordings of Brain Activity Using Organic Transistors. *Nat. Commun.* **2013**, *4*, 1575.
(19) Tarabella, G.; Nanda, G.; Villani, M.; Coppede, N.; Mosca, R.; Malliaras, G. G.; Santato, C.; Iannotta, S.; Cicoira, F. Organic Electrochemical Transistors Monitoring Micelle Formation. *Chem. Sci.* **2012**, *3*, 3432−3435.

DOI: 10.1021/acsami.7b07668
ACS Appl. Mater. Interfaces XXXX, XXX, XXX−XXX

(20) Liu, S.; Fu, Y.; Li, G.; Li, L.; Law, H. K.; Chen, X.; Yan, F. Conjugated Polymer for Voltage-Controlled Release of Molecules. *Adv. Mater.* **2017**, 1701733.
(21) *IUPAC Compendium of Chemical Terminology*; Nič, M., Jirát, J., Košata, B., Jenkins, A., McNaught, A., Eds.; IUPAC: Research Triagle Park, NC, USA, 2009.
(22) Long, G. L.; Winefordner, J. D. Limit of Detection A Closer Look at the IUPAC Definition. *Anal. Chem.* **1983**, *55*, 712A−724A.
(23) Khodagholy, D.; Rivnay, J.; Sessolo, M.; Gurfinkel, M.; Leleux, P.; Jimison, L. H.; Stavrinidou, E.; Herve, T.; Sanaur, S.; Owens, R. M.; Malliaras, G. G. High Transconductance Organic Electrochemical Transistors. *Nat. Commun.* **2013**, *4*, 2133.
(24) Tybrandt, K.; Kollipara, S. B.; Berggren, M. Organic Electrochemical Transistors for Signal Amplification in Fast Scan Cyclic Voltammetry. *Sens. Actuators, B* **2014**, *195*, 651−656.
(25) Rivnay, J.; Ramuz, M.; Leleux, P.; Hama, A.; Huerta, M.; Owens, R. M. Organic Electrochemical Transistors for Cell-Based Impedance Sensing. *Appl. Phys. Lett.* **2015**, *106*, 043301.
(26) Ramuz, M.; Hama, A.; Rivnay, J.; Leleux, P.; Owens, R. M. Monitoring of Cell Layer Coverage and Differentiation with the Organic Electrochemical Transistor. *J. Mater. Chem. B* **2015**, *3*, 5971−5977.
(27) Gualandi, I.; Tonelli, D.; Mariani, F.; Scavetta, E.; Marzocchi, M.; Fraboni, B. Selective Detection of Dopamine with an All PEDOT:PSS Organic Electrochemical Transistor. *Sci. Rep.* **2016**, *6*, 35419.
(28) Bernards, D. A.; Malliaras, G. G. Steady-State and Transient Behavior of Organic Electrochemical Transistors. *Adv. Funct. Mater.* **2007**, *17*, 3538−3544.
(29) Friedlein, J. T.; Donahue, M. J.; Shaheen, S. E.; Malliaras, G. G.; McLeod, R. R. Microsecond Response in Organic Electrochemical Transistors: Exceeding the Ionic Speed Limit. *Adv. Mater.* **2016**, *28*, 8398−8404.
(30) Huerta, M.; Rivnay, J.; Ramuz, M.; Hama, A.; Owens, R. M. Research Update: Electrical Monitoring of Cysts Using Organic Electrochemical Transistors a. *APL Mater.* **2015**, *3*, 030701.
(31) Pappa, A. M.; Inal, S.; Roy, K.; Zhang, Y.; Pitsalidis, C.; Hama, A.; Pas, J.; Malliaras, G. G.; Owens, R. M. Polyelectrolyte Layer-by-Layer Assembly on Organic Electrochemical Transistors. *ACS Appl. Mater. Interfaces* **2017**, *9*, 10427−10434.
(32) Proctor, C. M.; Rivnay, J.; Malliaras, G. G. Understanding Volumetric Capacitance in Conducting Polymers. *J. Polym. Sci., Part B: Polym. Phys.* **2016**, *54*, 1433−1436.
(33) Rivnay, J.; Leleux, P.; Ferro, M.; Sessolo, M.; Williamson, A.; Koutsouras, D. A.; Khodagholy, D.; Ramuz, M.; Strakosas, X.; Owens, R. M.; Benar, C.; Badier, J.-M.; Bernard, C.; Malliaras, G. G. High-Performance Transistors for Bioelectronics through Tuning of Channel Thickness. *Sci. Adv.* **2015**, *1*, e1400251.
(34) Liao, C. Z.; Zhang, M.; Niu, L. Y.; Zheng, Z. J.; Yan, F. Organic Electrochemical Transistors with Graphene-Modified Gate Electrodes for Highly Sensitive and Selective Dopamine Sensors. *J. Mater. Chem. B* **2014**, *2*, 191−200.

DOI: 10.1021/acsami.7b07668
ACS Appl. Mater. Interfaces XXXX, XXX, XXX−XXX